ACCOUNTS of chemical research

Article

pubs.acs.org/accounts

Light–Matter Interactions in Phosphorene

Junpeng Lu,[†,‡] Jiong Yang,[§] Alexandra Carvalho,[‡] Hongwei Liu,[*,∥] Yuerui Lu,[*,§] and Chorng Haur Sow[†,‡]

[†]Department of Physics, National University of Singapore, 2 Science Drive 3, 117542 Singapore

[‡]Center for Advanced 2D Materials and Graphene Research Center, National University of Singapore, 6 Science Drive 2, 117546 Singapore

[§]Research School of Engineering, College of Engineering and Computer Science, The Australian National University, Canberra, Australian Capital Territory 2601, Australia

[∥]Institute of Materials Research and Engineering, A*STAR (Agency for Science, Technology and Research), 2 Fusionopolis Way, Innovis, #08-03, 138634 Singapore

CONSPECTUS: Since the beginning of 2014, phosphorene, a monolayer or few-layer of black phosphorus, has been rediscovered as a two-dimensional (2D) thin film, revealing a plethora of properties different from the bulk material studied so far. Similar to graphene and transition metal dichalcogenides (TMDs), phosphorene is also a layered material that can be exfoliated to yield individual layers. It is one of the few monoelemental 2D crystals and the only one, besides graphene, known to be stable in monolayer, few layer, and bulk form. Recently the intensified research in phosphorene is motivated not only by the study of its fundamental physical properties in the 2D regime, such as tunable bandgap and anisotropic behavior, but also by the high carrier mobility and good on/off ratio of phosphorene-based device prototypes, making it a potential alternative for next generation nanooptoelectronics and nanophotonics applications in the "post-graphene age"

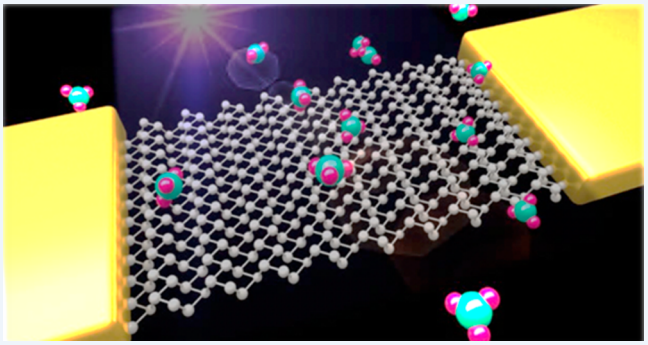

The electronic bandgap of phosphorene changes from 0.3 eV in the bulk to 2.1 eV in monolayer. Thus, phosphorene exhibits strong light–matter interactions in the visible and infrared (IR) frequencies. In this Account, we present the progress on understanding the various interactions between light and phosphorene, giving insight into the mechanism of these interactions and the respective applications. We begin by discussing the fundamental optical properties of phosphorene, using theoretical calculations to depict the layer-dependent electronic band structures and anisotropic optical properties. Many-body effects in phosphorene, including excitons and trions and their binding energies and dynamics are reviewed as observed in experiments. For phosphorene, the fast degradation in ambient condition, caused by photoinduced oxidation, is considered as a longstanding challenge. In contrast, oxidation can be used to engineer the band structure of phosphorene and, in parallel, its optical properties. Based on the strong light–matter interactions, we introduce a controllable method to directly oxidize phosphorene by laser techniques. With the oxidization induced by laser scanning, localized bandgap engineering can be achieved and microphotonics are demonstrated on the oxidized phosphorene.

Finally, we will present a brief discussion on the realization of phosphorene-based building blocks of optoelectronic devices. Naturally, the strong light–matter interactions in phosphorene could enable efficient photoelectric conversion in optoelectronic devices. We will describe high performance photodetectors based on phosphorene, and the working mechanism of those devices will be introduced. The photovoltaic effect could also be exhibited in phosphorene. This indicates the pervasive potential of phosphorene in nanooptoelectronics.

INTRODUCTION

Around 100 years ago, black phosphorus was successfully synthesized in the bulk form.[1] It is the most stable allotrope of phosphorus. Similar to graphite, black phosphorus is also a monotypic van der Waals layered crystal. Following the great upsurge in the research of 2D materials, black phosphorus in 2D form was recently revitalized and termed as phosphorene.[2−10] Due to the van der Waals layered structure, phosphorene can be readily produced by mechanical exfoliation. Different from graphene, which has zero bandgap, phosphorene has been found to have tunable direct bandgap. It was also demonstrated to present both high carrier mobility and high on/off ratio.[2]

Its thickness-dependent direct electronic bandgap makes phosphorene promising for nanophotonics and optoelectronics.[8,11−15] The performance of optoelectronic devices is significantly affected by factors such as light absorbance, photocarrier excitation, relaxation and separation, free carrier

Received: May 30, 2016

DOI: 10.1021/acs.accounts.6b00266
Acc. Chem. Res. XXXX, XXX, XXX−XXX

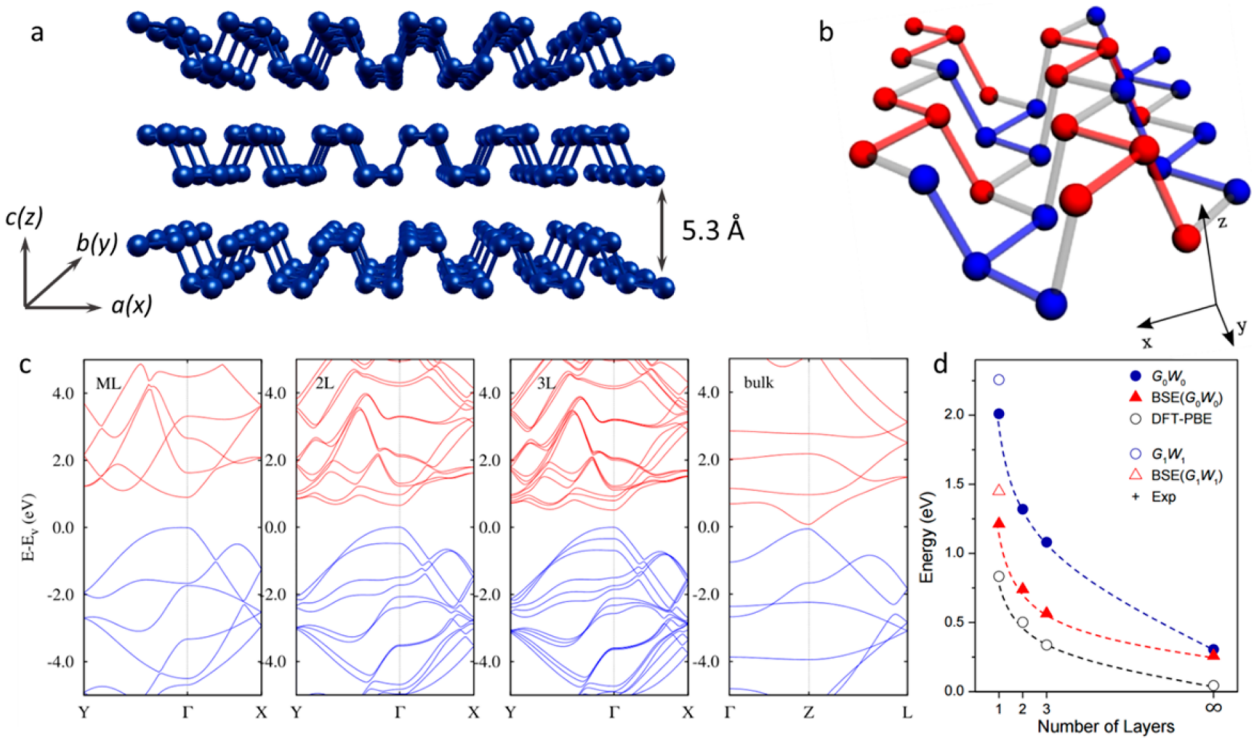

Figure 1. Crystal structure of phosphorene, (a) few-layer and (b) monolayer. (c) Calculated electronic band structures of phosphorene with different thicknesses. (d) The evolution of the electronic band gap as a function of layer number, calculated by different methods. Panel a adapted with permission from ref 15. Copyright 2016 John Wiley and Sons Panel b adapted with permission from ref 5. Copyright 2014 American Physical Society. Panel c adapted with permission from ref 56. Copyright 2014 American Physical Society. Panel d reprinted with permission from ref 20. Copyright 2014 American Physical Society.

diffusion, trapping/detrapping, and recombination.[16−18] All these are directly enabled, incidentally facilitated, or indirectly affected by light−matter interactions. Therefore, deep insight into light−matter interactions in phosphorene is desirable for the optimization of optoelectronic devices. In this Account, we discuss our recent efforts on the investigation of optical properties and photoelectrical properties of phosphorene. The discussion spans from fundamental theoretical calculations to experimental observations and devices. This Account is not meant to be a comprehensive review but is focused on discussing the unique optical features of phosphorene, such as tunable direct bandgap, quasi-1D excitons, anisotropic luminescence, and vibrational properties.

■ ELECTRONIC BAND STRUCTURE

Black phosphorus has a puckered orthorhombic lattice structure obeying the D_{2h}^{18} space group symmetry. The interlayer spacing between two single-layers is 0.53 nm (Figure 1a). The unit cell contains four atoms with two symmetry-inequivalent P−P bonds (Figure 1a,b). Each phosphorus atom connects to three neighboring atoms.

The interesting optical properties of 2D semiconductors arise from the electronic structure and dispersion of the electronic states at the 2D limit. The calculated electronic band structures of phosphorene with different thickness are shown in Figure 1c. Different from the indirect to direct bandgap transition in transition metal dichalcogenides (TMDs) from bulk to monolayer, the bandgap of phosphorene remains direct for any number of layers. However, the conduction band minimum (CBM) and valence band maximum (VBM) coincide at the Z point in bulk black phosphorus, but they shift to the Γ point when the thickness is reduced to few layer and monolayer. Remarkably, the valence band top of the monolayer phosphorene is very flat. Possibly the VBM might even be slightly off the Γ point.[19] But the monolayer phosphorene is still approximately considered as direct bandgap since the separation between the VBM and Γ point is less than 10 meV.[20] The theoretical evolution of the bandgap according to the layer numbers is shown in Figure 1d. The estimated bandgap of the phosphorene varies from around 2.0 eV in monolayer to around 0.3 eV in bulk, consistent with the experimental results. Liang et al. measured a bandgap of 2.05 eV for phosphorene monolayer through scanning tunneling microscope (STM) characterization,[21] and Xia et al. estimated the bandgap of bulk black phosphorus to be ∼0.3 eV from the infrared relative extinction spectra.[8] The range of the tunable bandgap makes phosphorene present photoresponse covering the visible to IR spectral regime (Figure 2a). This fills the void of the 2D materials where graphene has zero bandgap[22,23] and group VI TMDs mostly show response in the visible spectrum.[24] In addition, changes in the local geometry such as tensile and compressive strain and curvature could be employed to further modify the band structure of phosphorene,[5,25−27] for example, inducing a metal−semiconductor transition (Figure 2b). As a result, phosphorene's interaction with light can cover a very broad spectral range.

As a consequence of its puckered orthorhombic lattice structure with the D_{2h} symmetry, phosphorene exhibits in-plane anisotropy.[6,8,28] The difference the effective mass of carriers along the zigzag direction (y) is ∼10 times heavier than that along the armchair direction (x).[10,29] At the optical aspect, the anisotropy is determined by the optical selection rules. The occurrence of the optical transition relates to the momentum

DOI: 10.1021/acs.accounts.6b00266
Acc. Chem. Res. XXXX, XXX, XXX−XXX

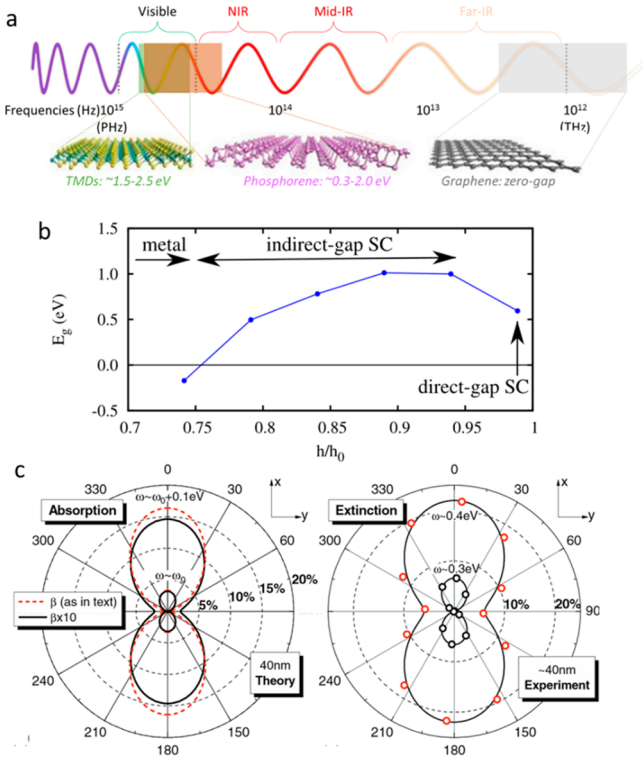

Figure 2. (a) Spectral response range of the band gaps of various types of 2D materials. (b) Band gap versus the height h (corresponds to the applied strain) for phosphorene. The original layer thickness is $2h_0$. (c) (left) Predicted angle-dependent absorption coefficient $A(\alpha)$, where α is the light polarization angle; (right) experimental measured angle-dependent extinction spectra. Panel b adapted with permission from ref 5. Copyright 2014 American Physical Society. Panel c adapted with permission from ref 56. Copyright 2014 American Physical Society.

operator, $\hat{p}_{x/y}$.[19] In phosphorene monolayer, the $\hat{p}_x$ matrix element between VBM and CBM is finite, allowing electronic transitions, while the $\hat{p}_y$ matrix element is zero so that transitions with y-polarization are forbidden by symmetry.[30] The anisotropy of the absorption coefficient, as found by theoretical calculations, highlights how markedly it depends on the polarization angle (Figure 2c). The calculation result agrees well with the experimentally measured extinction spectra, which include information on both light absorption and reflection of a phosphorene sample. Since the anisotropy of the optical properties is very significant, it can be used to determine the crystallographic axes.

EXCITONIC EFFECTS

The evolution of the electronic band structure and induced optical property in phosphorene has been monitored by collection of the excitonic emissions using photoluminescence (PL) spectroscopy. The normalized PL spectra of phosphorene with varying thickness are shown in Figure 3a. The significant blue-shift of the peak position clearly indicates the widening of the bandgap with decreasing thickness. The broadness arises from the synergy of the quantum confinement effect and the interactions between the layers.[20,31] In addition to the peak shift, the PL intensity is also observed to significantly increase with decreasing layer numbers.[32] The enhancement is due to the decreasing of the density of states at the valley extrema. They can increase the relaxation rates of carriers and lower the internal quantum efficiency.

The optical gap, E_{opt}, can be estimated from the PL peak position. Accordingly, the E_{opt} of phosphorene with thickness from monolayer to five layers are ~1.75, ~1.29, ~0.97, ~0.84 and ~0.80 eV, respectively. The spectra are collected on the mechanically exfoliated samples on SiO_2/Si substrate. These experimental values can be described well by a power law formula, $E_{opt} = 1.486/N^{0.686} + 0.295$, where N is the number of layers (Figure 3b). The variation trend of the optical gap as a function of layer numbers is consistent with the theoretical prediction.[6,20] However, the obtained values of the optical gaps are smaller than the electronic bandgaps (E_g).[20,21] This is caused by the exciton binding energy (E_b) in phosphorene. E_b can be calculated from the difference between E_g and E_{opt}, as illustrated by the schematic in the inset of Figure 3b,d. By employing the experimentally measured E_g of ~2.05 eV for phosphorene monolayer, the E_b of phosphorene monolayer can be estimated to be ~0.3 eV, which is well consistent with the theoretical prediction, taking into account that dielectric substrate, capping layer, and contacts, if present, provide increased screening, reducing E_b (Figure 3c). Due to the strong quantum confinement effect, the isolated phosphorene monolayer is predicted to have a large E_b of 0.76 eV using the numerical calculation methods.[28] The large value of E_b indicates the high stability of excitons in phosphorene. It arises from the strong confinement of electrons and holes and the reduced screening of the Coulomb interaction. Consequently, the optical properties of phosphorene are dominated by excitons. Furthermore, E_b of phosphorene could be further increased when subjected to a uniaxial transverse strain (Figure 3e). It is predicted to be as high as 0.87 eV for 5% strain. This value is even comparable to the quasiparticle bandgap of phosphorene and is the highest among 2D materials (Figure 3f).

The quantum confinement effect and reduced dielectric screening in 2D systems lead to carrier Coulomb interactions. This is the main reason for the tightly bound exciton while it can also lead to higher-order excitonic states, for example, charged excitons (termed trions). A trion consists of two electrons (holes) and one hole (electron). After the observation of strongly bound trions in 2D TMDs, there is fast growing interest in the investigation of trions for fundamental studies of many-body interactions, spin manipulation, carrier multiplication, etc.[33−35] The many-body bound trion state arises from the interaction of an exciton with a free carrier. By controlling the doping level, the density of trions can be modulated. Electrostatic modulation and photocarrier injection have been demonstrated as effective methods to modulate the trions.[36,37] Based on a FET device, the exciton charging effects in phosphorene trilayer can be gradually tuned from positive to neutral through changing the gate voltage, as monitored by the PL spectra (Figure 4a). The relative intensity of the exciton emission (~1100 nm) and the trion emission (~1300 nm) is sensitive to the applied gate voltage. When negative gate bias is applied, positive charges are injected into phosphorene. In doing so, trion emission dominates the PL emission. In contrast, trion emission becomes weaker when positive gate bias is applied. The optical tunability of trions has been demonstrated in phosphorene monolayer.[37] The binding energy of trion can be approximately estimated from the energy difference of exciton and trion. The difference represents the minimum energy required to remove an electron (hole) from a negative (positive) trion.[38] Therefore, the binding energies of trion in phosphorene monolayer and trilayer are measured to be ~100 and ~160 meV, respectively. These values are much larger than those measured at other 2D systems such as the quantum

DOI: 10.1021/acs.accounts.6b00266
Acc. Chem. Res. XXXX, XXX, XXX−XXX

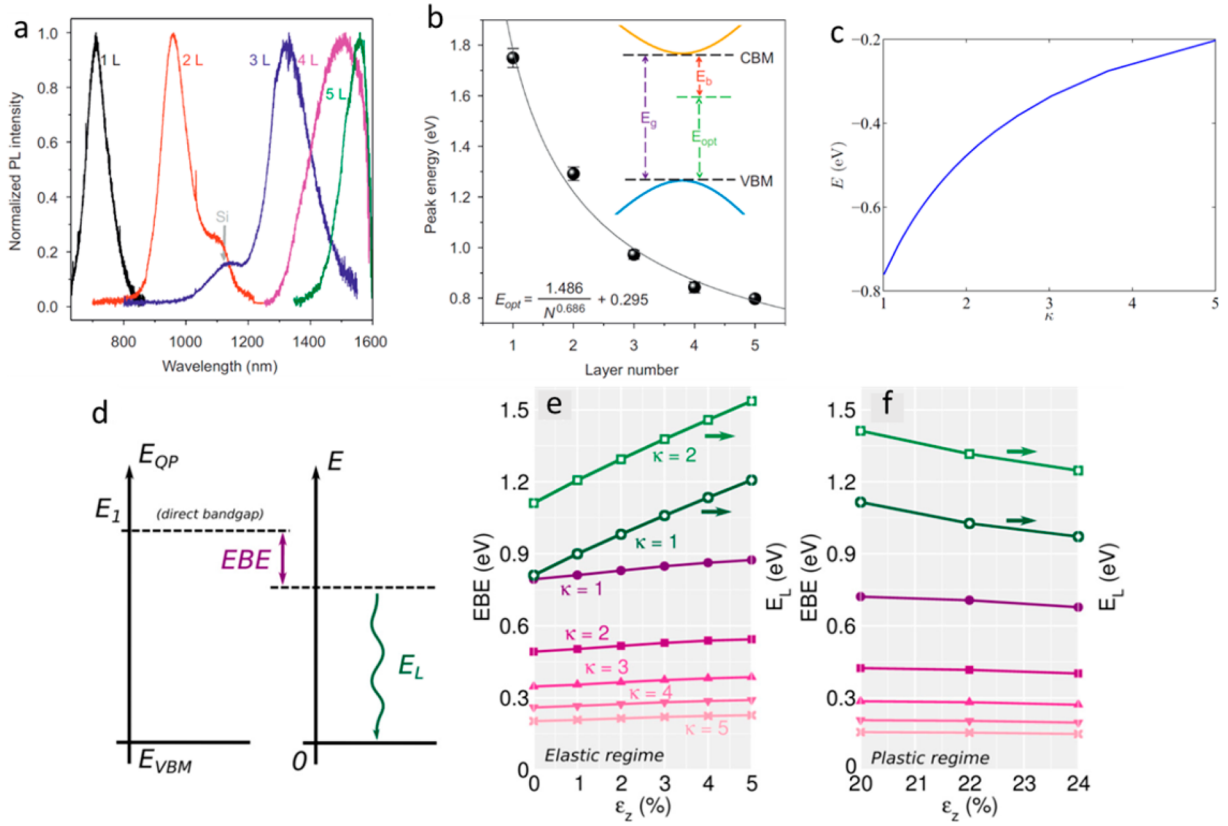

Figure 3. (a) Normalized PL spectra of phosphorene with varying thickness. (b) E_{opt} as a function of layer number. Inset shows the schematic illustration of the electronic band gap and exciton binding energy. (c) Exciton binding energy as a function of dielectric constant, κ. (d) Energy diagram of the band gap, binding energy (EBE), and photon energy (E_L). (e, f) Emitted photon energy and exciton binding energy as a function of strain, ε_z. Panels a and b adapted with permission from ref 37. Copyright 2015 Nature Publishing Group. Panel c adapted with permission from ref 28. Copyright 2014 American Physical Society. Panels d–f adapted with permission from ref 57. Copyright 2015 American Physical Society.

wells and TMDs and are comparable to the trions in 1D systems such as carbon nanotubes.[39]

The high amplitude of the trion binding energy in phosphorene arises from its anisotropic nature. The excitons and trions are predicted to be confined in a quasi-1D space in phosphorene. The quasi-1D characteristics can be validated by detection of completely linearly polarized exciton and trion emissions by angle-resolved PL spectroscopy. The diagram of the setup is shown in Figure 4b. First, the PL intensity depends on the polarization of the excitation light (θ_1) (Figure 4c). This is due to the anisotropic absorption of phosphorene. If a certain polarization direction is fixed, the emissions from excitons and trions are observed to be completely linearly polarized along the armchair direction (Figure 4d,e).

PLASMONS

Plasmons are collective excitations of a system, characterized by zeros of the real part of the dielectric constant. Plasmons have been studied in undoped[40] and doped[41] phosphorene. In doped phosphorene, both intraband and interband transitions are possible. As a result, the real part of the components of the permittivity tensor have opposite signs in a certain frequency range. Such material is termed hyperbolic, because of the hyperboloid topology of the dispersion relation in k-space. Therefore, plasmons in that frequency range propagate as a localized beam along the direction defined by the ratio of the imaginary parts of the optical conductivity. Manifestation of the hyperbolic regime may be inhibited by nonlocality.

VIBRATIONAL PROPERTIES

The phonon modes at the Γ point in phosphorene belong to the representation $2A_g + B_{1g} + B_{2g} + 2B_{3g} + A_u + 2B_{1u} + 2B_{2u} + B_{3u}$. Among these modes, B_{1u}, B_{2u}, and B_{3u} are acoustic modes and all the rest even parity modes are Raman active modes.[42] Generally, three prominent Raman peaks at around ~362.3, 438.9, and 467.3 cm^{-1}, ascribed to the irreducible representations of A_g^1, B_{2g}, and A_g^2 phonon modes,[15] respectively, can be observed in the Raman spectrum (Figure 5a). The vibration of the A_g^1, B_{2g}, and A_g^2 modes oscillate along the *z*, *y*, and *x* directions, respectively (Figure 5b). Different from TMDs, the Raman spectra are not usually regarded as the unambiguous signature of layer number of phosphorene since the frequency of the phonon modes is not significantly dependent on the layer number.[43] Especially, the shifts of A_g^1 and B_{2g} are negligible (<1 cm^{-1}).[44] This is consistent with the theoretical prediction that the variation of the lattice parameter along the *y* direction with the layer number is insignificant.[6] The broadening of the width of the Raman peaks is observed in phosphorene few-layers with the decreasing of the layer number. It reaches the maximum at trilayer and shrinks back at the monolayer. This is due to the larger number of P atoms at the primitive cell in phosphorene few-layers where the primitive cells consist of 4*n* atoms. It is larger than the four-atom primitive cell of phosphorene monolayer and bulk. The large number of atoms in a unit cell can induce Davydov splitting and give rise to the broadening of the photon modes.[44]

DOI: 10.1021/acs.accounts.6b00266
Acc. Chem. Res. XXXX, XXX, XXX−XXX

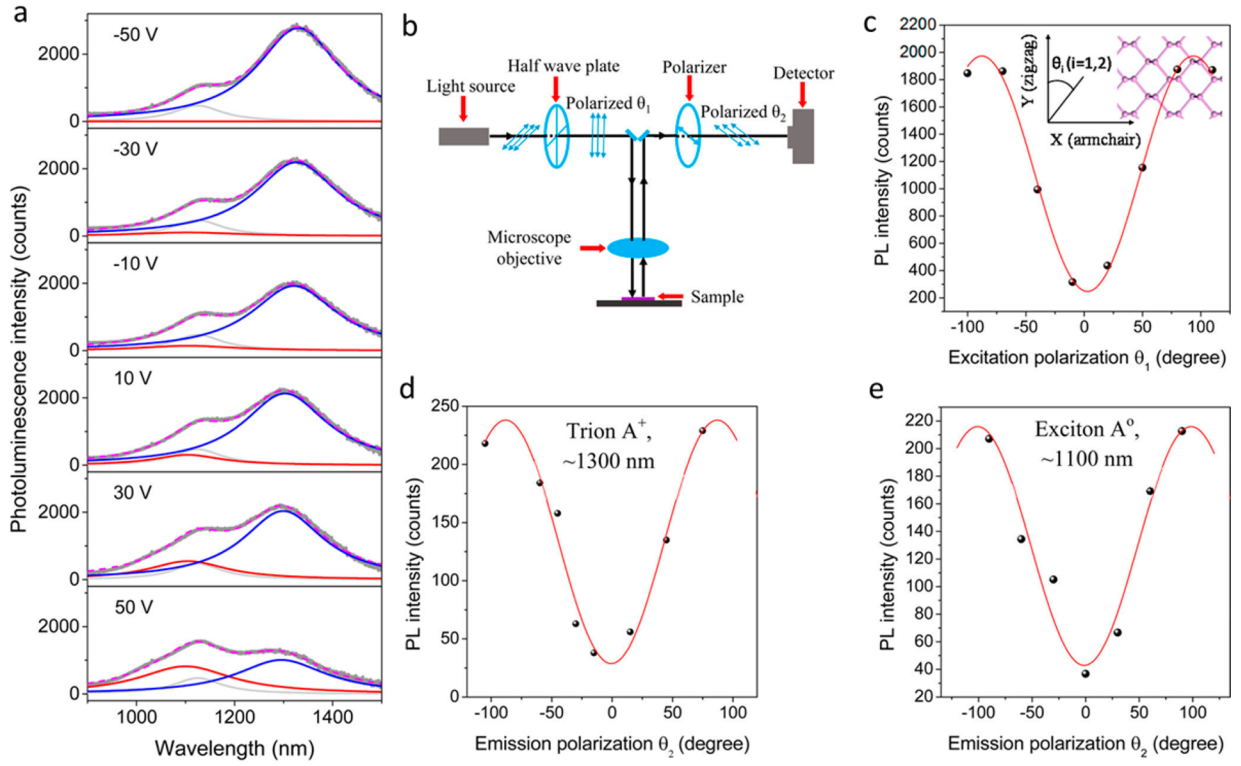

Figure 4. (a) Gate tunability of excitons and trions in phosphorene trilayer. (b) Schematic illustration of the setup used for polarization dependent PL measurement. (c) Intensity of trion emission as a function of excitation polarization. Intensity of (d) trion and (e) exciton emission as a function of emission polarization. Adapted with permission from ref 36. Copyright 2016 American Chemical Society.

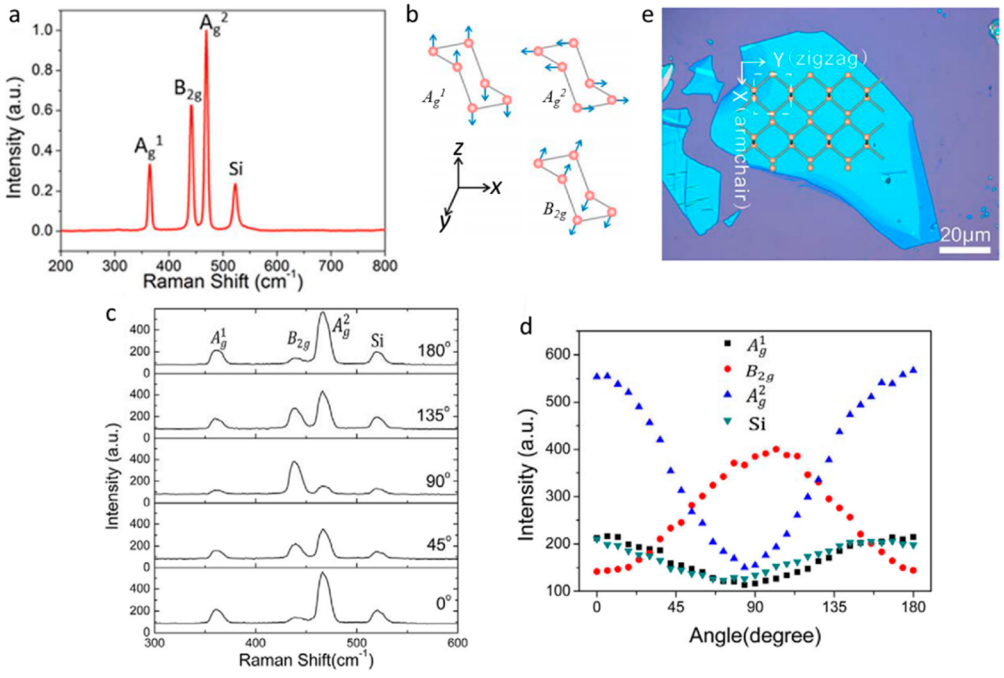

Figure 5. (a) Raman spectrum of a typical phosphorene sample. (b) Schematic illustration of the vibration modes. (c) Raman spectra of a phosphorene sample collected at different polarization angles. (d) Intensities of the Raman peaks as a function of polarization angle. (e) Determination of crystalline orientation via polarization-dependent Raman spectra. Panel a adapted with permission from ref 15. Copyright 2016 John Wiley and Sons. Panels b–e adapted with permission from ref 32. Copyright 2014 American Chemical Society.

Despite of the fact that the Raman peaks do not show very significant dependence on the layer number, their intensity exhibits strong dependence on the polarization angle (Figure 5c) due to anisotropy of phosphorene. Peak intensities of B_{2g} and A_g^2 display opposite variation with changes in the polarization angle, and the angular period is 180° (Figure 5d). However, the intensity of A_g^1 is not sensitive to the angle.[14,32] Since the vibration of A_g^1 is out-of-plane, it does not vary with the laser

DOI: 10.1021/acs.accounts.6b00266
Acc. Chem. Res. XXXX, XXX, XXX−XXX

polarization. When the laser polarization is parallel to the armchair direction along which the A_g^2 mode oscillates, the intensity of A_g^2 reaches its maximum. When the laser polarization is parallel to the zigzag direction along which the B_{2g} mode oscillates, the intensity of B_{2g} reaches its maximum. Accordingly, polarization-resolved Raman spectroscopy can be used as a fast and precise way to determine the crystalline orientation of phosphorene (Figure 5e).

DEFECT ENGINEERING

Defects can introduce extra electronic states in the bandgap thus significantly influencing the carrier transfer in the material and render different light−matter interactions. Therefore, deep insight into the functionalities and precise control of the defects provides the possibility of manipulating light−matter interactions in 2D semiconductors. Since the degradation of phosphorene is mainly caused by surface reactions with oxygen, oxygen chemisorption/physisorption is predicted to be the fundamental cause of neutral and electrically active defects in phosphorene.[45] When the phosphorene is subjected to oxygen plasma or light pumping, where the oxygen source is more active than its ground state, bridge-type (including horizontal and diagonal bridges (Figure 6a,b) surface oxygen defects would be generated. These defect states are predicted to serve as recombination centers to generate photon emissions.[45] Oxygen plasma etching provides more reactive conditions where oxygen defects might be introduced and controlled in phosphorene.[46] By carefully controlling the oxygen flow rate, plasma generation power, and etching time, high-quality phosphorene monolayer can be fabricated. It presents higher PL intensity than the exfoliated monolayer due to the well-protected surface by a stable P_xO_y layer (Figure 6c). The PL peak at 750 nm is ascribed to trion emission.[37] When the phosphorene monolayer is over etched with oxygen plasma, two strong PL peaks can be observed at 780 and 915 nm, respectively. The spectrum is fitted by two Gaussian curves (P_1 and P_2). The integrated intensities of both P_1 and P_2 increase sublinearly with increasing excitation power. This indicates that these two peaks arise from the emissions from excitons localized onto the oxygen defects. As indicated by calculated energy diagrams shown in Figure 6a,b, P_1 and P_2 can be attributed to the emissions from excitons bonded to horizontal and diagonal bridge oxygen defects, respectively. In addition, the broad width of the peaks indicates that there might be contributions from other kinds of defects such as dangling oxygen, interstitial oxygen, physisorbed oxygen, water, etc.[45] Remarkably, the intensity of P_1 and P_2 can be tuned by applying electrical gate (Figure 6d). The PL intensity increases when the gate voltage is swept from 50 to −50 V. This indicates the initial n-type behavior of the phosphorene monolayer with oxygen defects. Given the p-type behavior of the pristine phosphorene, oxygen defect engineering can be employed as effective way to convert the doping behavior in phosphorene. Aside from using oxygen plasma, oxygen defects can also be introduced to phosphorene by engineering the substrate. By transfer of monolayer phosphorene onto plasma-enhanced chemical vapor deposition (PECVD)-fabricated SiO_x substrate, interfacial luminescent local states are formed. They can capture free excitons in phosphorene to generate 0D-like localized excitons, resulting in efficient photon emission at ∼920 nm.[47] The quantum yield of localized excitons is calculated to be 33.6 times larger than that of free excitons.

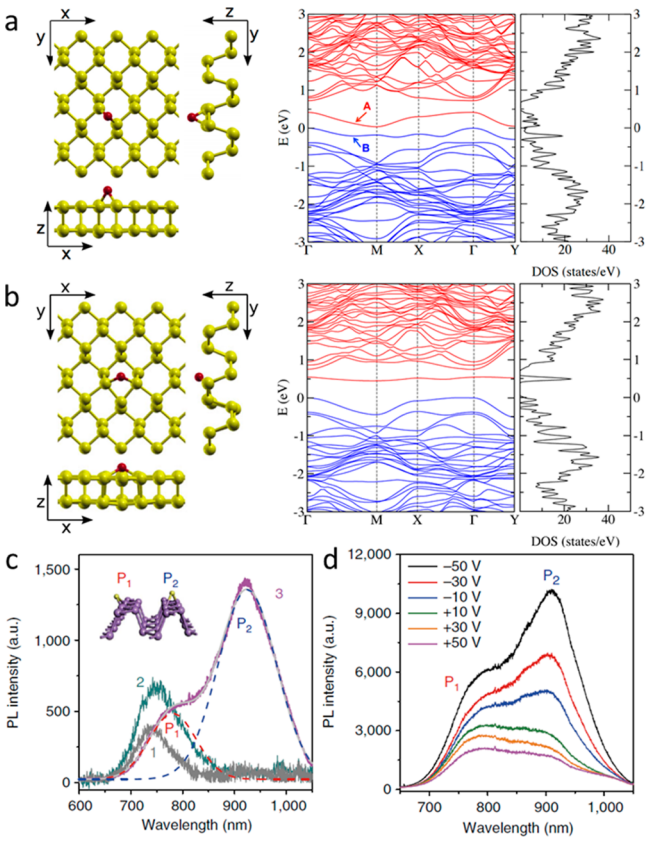

Figure 6. (a) Diagonal and (b) horizontal oxygen bridge. From left to right, projections of structure, electronic structure, and DOS. (c) PL spectra of (1) exfoliated phosphorene monolayer, (2) phosphorene monolayer fabricated by oxygen plasma etching, and (3) phosphorene monolayer with over etching. Inset shows the schematic illustration of the diagonal and horizontal oxygen bridge defects. (d) PL spectral of sample 3 under different gate voltages. Panels a and b adapted with permission from ref 45. Copyright 2015 American Physical Society. Panels c and d adapted with permission from ref 46. Copyright 2016 Nature Publishing Group.

BANDGAP ENGINEERING VIA OXIDATION

Given the tendency to oxidize, the properties of phosphorene degrade significantly even within half an hour after preparation.[48−50] The tendency toward oxidation is caused by the electron lone pairs at the surface of phosphorene, which can work as a preferred site to bond to oxygen atoms.[45] To weaken the influence of the oxidation, researchers dedicated 2 years of effort to understand the mechanisms of the oxidation and ultimately prevent it.[51] Instead of fighting the oxidation as a detriment, a controlled oxidation process can lead to a protective layer to preserve the phosphorene underneath or a functional material of its own.[52,53] The bandgaps of phosphorene oxides (P_4O_n) strongly depend on the oxygen concentration. This makes it feasible to engineer the bandgap of phosphorene by oxidation. The wide range of the tunable bandgap extends the spectral regime of the light−matter interactions in phosphorene from visible to deep UV. Each P_4O_n with certain oxygen concentration has two distinctive classes of 2D planar (p-P_4O_n) and 1D tubular (t-P_4O_n) forms. Considering the large surface area of the 2D phosphorene, surface form (s-P_4O_n) is also identified. The crystal structures of representative suboxides are shown in Figure 7a. The electronic band structure of phosphorene significantly changes with the degree of oxidation. The bandgap of p-P_4O_n is predicted to monotonically increase with oxygen concentration

DOI: 10.1021/acs.accounts.6b00266
Acc. Chem. Res. XXXX, XXX, XXX−XXX

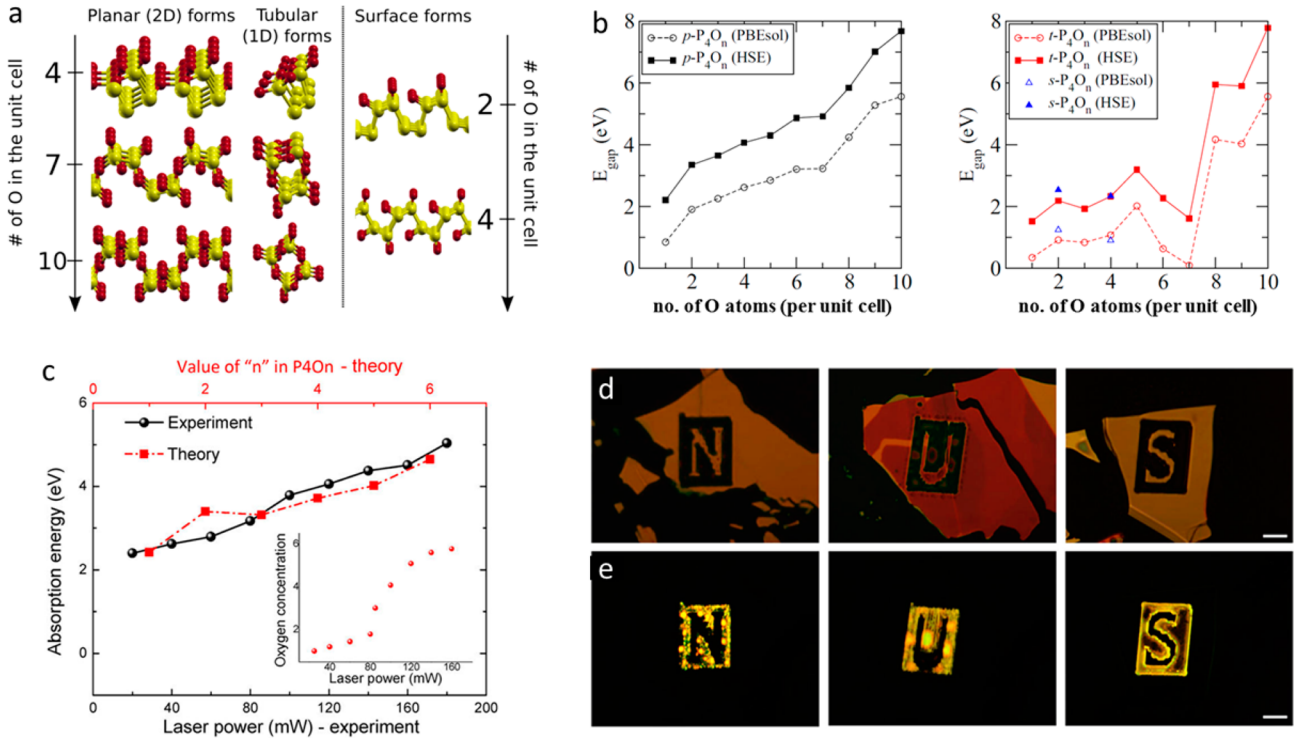

Figure 7. (a) Crystal structures of different forms of phosphorene oxides. (b) Calculated bandgap using different methods as a function of oxygen concentration. (c) Bandgap as a function of laser power (experimental result) and oxygen concentration (theoretical calculation). Inset shows the "calibration" map of oxygen concentration as a function of laser power. (d) Optical and (e) fluorescent images of the phosphorene oxides. Panels a and b adapted with permission from ref 58. Copyright 2015 American Physical Society. Panels c–e adapted with permission from ref 53. Copyright 2014 American Chemical Society.

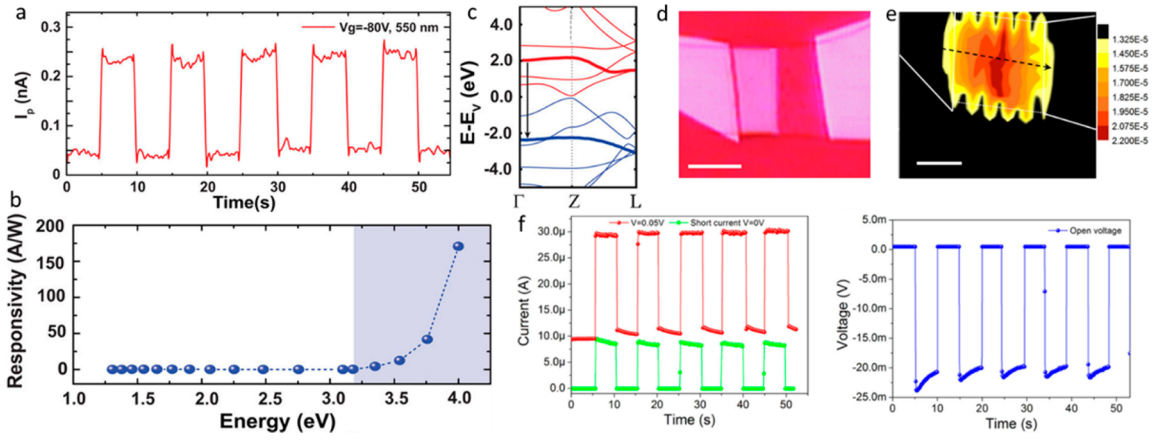

Figure 8. (a) Photoresponse of phosphorene device to light with wavelength of 550 nm. (b) Photoresponsivity as a function of incident photon energy, measured at $V_g = -80$ V and $V_{sd} = 0.1$ V. (c) Band structure of phosphorene. Band nesting is indicated by arrow. (d) Optical image and (e) photocurrent map of a phosphorene–phosphorene suboxide device. Left part of the phosphorene film is converted into phosphorene suboxide by a scanning focused laser beam. (f) (left) Photoresponse of phosphorene–phosphorene suboxide device to light with wavelength of 532 nm at a bias of 0.05 and 0 V; (right) photogenerated voltage. Panels a–c adapted with permission from ref 14. Copyright 2015 American Chemical Society. Panel d–f adapted with permission from ref 15. Copyright 2016 John Wiley and Sons.

(Figure 7b). It changes from ~0.9 eV ($n = 1$) to ~5.5 eV ($n = 10$) under the PBEsol calculation method. Similarly, the bandgap of t-P_4O_n is also predicted to increase with oxygen concentration. The broadening of the bandgap arises from the increase of the ionic character of the bonds and the induced localization of wave function.[45] From the calculations, the energy difference between p-P_4O_n and t-P_4O_n is small (<0.1 eV per O atom). Therefore, both forms will coexist under normal oxidizing conditions. Ordered and amorphous domains might be formed depending on the fabrication process. Light–matter interactions enabled by lasers with high power intensity would trigger complex and interesting phenomena, such as photodestruction or modification, photochemical reaction, or photo-oxidation. A photo-oxidation technique based on a focused laser beam has been devised to controllably fabricate phosphorene suboxides.[53] Upon this technique, suboxides can be locally created on the phosphorene with well-defined micropatterns (Figure 7d). The bandgap of the suboxides could be flexibly engineered from ~2.3

DOI: 10.1021/acs.accounts.6b00266
Acc. Chem. Res. XXXX, XXX, XXX–XXX

to ∼5.1 eV by controlling the laser power, consistent with the theoretical calculations (Figure 7c). The fabricated suboxides are observed to be photoactive in the visible regime and present fluorescence emissions (Figure 7e).

OPTOELECTRONIC DEVICES

Photoelectrical conversion is generally considered as the basis of the optoelectronic devices. Invariably, the strong light−matter interactions presented in phosphorene confer the flexibility of photoelectrical energy conversions. Next generation optoelectronic devices have special demands, transparency, lightweight, wearability, etc. Two-dimensional phosphorene can readily satisfy such requirements due to its transparency, mechanical flexibility, and other advantages for device integration. An optoelectronic device is normally used to detect or generate light. For light detection, generation of photocurrent upon photoelectrical conversion renders the operation of a photodetector. The tunable direct bandgap of phosphorene makes it a promising building block of a photodetector with multispectral response from UV to NIR regime. The photodetector based on phosphorene presents very fast response under the irradiation of visible light (550 nm) (Figure 8a). The photoresponsivity is calculated to be ∼1.82 A W^{-1}. The performance of the device improves for detecting UV light. The photoresponsivity increases with the photon energy and reaches its maximum of ∼175 A W^{-1} at a bias of 0.1 V (Figure 8b). It can be even increased to $\sim 9 \times 10^4$ A W^{-1} at higher bias of 3 V. This is 4-fold higher than that in the visible and NIR regime, offering phosphorene potential as a UV detector. Another important parameter, specific detectivity, is calculated to be $\sim 3 \times 10^{13}$ Jones [cm $Hz^1/2W^{-1}$]. It is comparable to other higher performance UV detectors.[54,55] The high responsivity in the UV regime arises from the large absorption of the UV light caused by the band nesting (Figure 8c), that is, the existence of a region in the band structure where the conduction band and the valence band are parallel, which have a diverging optical conductivity. The photogenerated electrons and holes at the band nesting present velocities with same amplitude but opposite direction. Thus, the electron−hole pairs prefer to separate and generate higher photocurrent.

Optoelectronic devices based on photovoltaic effect are operated by the photoelectrical conversion realized in built-in electric fields, for example, in p−n junctions. Electrostatically doping by local gate has been developed to introduce a p−n junction in phosphorene with the aim to increase the photoresponse. However, the complexity of the fabrication of local gate electrodes is viewed as an impediment for applications. Alternatively, connection of phosphorene with phosphorene oxides could also form a functional junction with the capacity to induce a built-in electric field. As described above, a scanning focused laser beam can be used locally to create phosphorene oxides/suboxides on the phosphorene, thus creating a functional junction in situ (Figure 8d), which has higher response to light (maximum photocurrent) than the original phosphorene (Figure 8e). Moreover, "photovoltaic-like" behavior is shown by the junction. Under the irradiation of light with power of 4.2 mW, the photogenerated voltage and output short-circuit current are measured to be ∼20 mV and ∼10 μA, respectively (Figure 8f).

CONCLUSIONS AND PROSPECTS

Light−matter interactions are generally considered as the basis of optoelectronics in condensed matter physics. While overviewing the optical and photoelectrical properties of phosphorene, we focused on three main aspects to provide a concise account to describe the concepts where the light−matter interactions could be triggered, observed, and implemented. First, the structure of phosphorene renders anisotropic fundamental optical phenomena. The tunable direct bandgap extends the spectral range of the photoresponse. Strong excitonic effects have potential application for light emissions. Simultaneously, we discussed how optical properties of phosphorene can be modified by oxidation. Oxygen chemisorption/physisorption is predicted to be one source of defects with bandgap states in phosphorene. These states may provide the possibility to manipulate the light−matter interactions in phosphorene. On the other hand, controllable oxidation of phosphorene could be realized by a special way of light−matter interaction. That is based on the photochemical reaction induced by pruning phosphorene using a focused laser beam. Thus, one can engineer the bandgap of phosphorene by controlling the degree of oxidation. Finally, the strong light−matter interactions give rise to the implementation in optoelectronics. Especially, the anisotropy makes phosphorene more versatile in light generation, manipulation, and detection.

The fast degradation in ambient conditions is the main bottleneck of using phosphorene in practical applications at present. Therefore, suitable encapsulation is desired. Encouraging results have been demonstrated from the encapsulations by deposition of insulating materials of Al_2O_3, PMMA, and BN on phosphorene to isolate oxygen and water. In addition, in situ oxidation of the top layers can work as the protective layer of the underneath phosphorene. Until now, many interesting research activities demonstrate novel optical properties and promising potential for phosphorene in optoelectronics, but most of the studies on the light−matter interactions in phosphorene are still in infancy, and many of its capacities may still be untapped. For example, the strong light−matter interactions and anisotropy may lead to the interesting studies of plasmons and polaritons. Furthermore, transdisciplinary collaboration is required to access the applications of phosphorene in different scientific fields.

AUTHOR INFORMATION

Corresponding Authors

*E-mail: liuhw@imre.a-star.edu.sg.
*E-mail: yuerui.lu@anu.edu.au.

Notes

The authors declare no competing financial interest.

Biographies

Dr. Junpeng Lu received his Ph.D. from National University of Singapore (NUS) and currently is a Research Fellow at NUS. His research interest lies in nanophotonics and optoelectronics.

Mr. Jiong Yang is a Ph.D. student of NEMS lab in Australian National University (ANU). His research interests include 2D materials, nanophotonics, and device design based on 2D materials.

Dr. Alexandra Carvalho joined NUS Centre for Advanced 2D Materials and Graphene Centre in 2013. Her research is focused on modeling of defects and nanostructures using density functional theory.

Dr. Hongwei Liu received her Ph.D. from NUS. She joined Institute of Materials Research and Engineering, A*STAR, Singapore, as Research Scientist. Her research focuses on the spectroscopy characterization of nanomaterials.

Dr. Yuerui Lu is a Senior Lecturer and group leader of NEMS Lab at ANU. His research interests include MEMS/NEMS, nanomanufactur-

DOI: 10.1021/acs.accounts.6b00266
Acc. Chem. Res. XXXX, XXX, XXX−XXX

ing, renewable energy harvesting, biomedical novel devices, and 2D materials.

Dr. Chorng Haur Sow is a Professor at NUS. His research is focused on laser−matter interactions for low-dimensional materials and the development of laser pruning methods for nanostructures.

REFERENCES

(1) Bridgman, P. W. Two new modifications of phosphorus. *J. Am. Chem. Soc.* **1914**, *36*, 1344−1363.
(2) Li, L.; Yu, Y.; Ye, G. J.; Ge, Q.; Ou, X.; Wu, H.; Feng, D.; Chen, X. H.; Zhang, Y. Black phosphorus field-effect transistors. *Nat. Nanotechnol.* **2014**, *9*, 372−377.
(3) Liu, H.; Neal, A. T.; Zhu, Z.; Luo, Z.; Xu, X.; Tománek, D.; Ye, P. D. Phosphorene: An unexplored 2d semiconductor with a high hole mobility. *ACS Nano* **2014**, *8*, 4033−4041.
(4) Koenig, S. P.; Doganov, R. A.; Schmidt, H.; Castro Neto, A. H.; Özyilmaz, B. Electric field effect in ultrathin black phosphorus. *Appl. Phys. Lett.* **2014**, *104*, 103106.
(5) Rodin, A. S.; Carvalho, A.; Castro Neto, A. H. Strain-induced gap modification in black phosphorus. *Phys. Rev. Lett.* **2014**, *112*, 176801.
(6) Qiao, J.; Kong, X.; Hu, Z.-X.; Yang, F.; Ji, W. High-mobility transport anisotropy and linear dichroism in few-layer black phosphorus. *Nat. Commun.* **2014**, *5*, 4475.
(7) Churchill, H. O. H.; Jarillo-Herrero, P. Two-dimensional crystals: Phosphorus joins the family. *Nat. Nanotechnol.* **2014**, *9*, 330−331.
(8) Xia, F.; Wang, H.; Jia, Y. Rediscovering black phosphorus as an anisotropic layered material for optoelectronics and electronics. *Nat. Commun.* **2014**, *5*, 4458.
(9) Liu, H.; Du, Y.; Deng, Y.; Ye, P. D. Semiconducting black phosphorus: Synthesis, transport properties and electronic applications. *Chem. Soc. Rev.* **2015**, *44*, 2732−2743.
(10) Ling, X.; Wang, H.; Huang, S.; Xia, F.; Dresselhaus, M. S. The renaissance of black phosphorus. *Proc. Natl. Acad. Sci. U. S. A.* **2015**, *112*, 4523−4530.
(11) Deng, Y.; Luo, Z.; Conrad, N. J.; Liu, H.; Gong, Y.; Najmaei, S.; Ajayan, P. M.; Lou, J.; Xu, X.; Ye, P. D. Black phosphorus−monolayer mos2 van der waals heterojunction p−n diode. *ACS Nano* **2014**, *8*, 8292−8299.
(12) Buscema, M.; Groenendijk, D. J.; Steele, G. A.; van der Zant, H. S. J.; Castellanos-Gomez, A. Photovoltaic effect in few-layer black phosphorus pn junctions defined by local electrostatic gating. *Nat. Commun.* **2014**, *5*, 4651.
(13) Buscema, M.; Groenendijk, D. J.; Blanter, S. I.; Steele, G. A.; van der Zant, H. S. J.; Castellanos-Gomez, A. Fast and broadband photoresponse of few-layer black phosphorus field-effect transistors. *Nano Lett.* **2014**, *14*, 3347−3352.
(14) Wu, J.; Koon, G. K. W.; Xiang, D.; Han, C.; Toh, C. T.; Kulkarni, E. S.; Verzhbitskiy, I.; Carvalho, A.; Rodin, A. S.; Koenig, S. P.; Eda, G.; Chen, W.; Neto, A. H. C.; Özyilmaz, B. Colossal ultraviolet photoresponsivity of few-layer black phosphorus. *ACS Nano* **2015**, *9*, 8070−8077.
(15) Lu, J.; Carvalho, A.; Wu, J.; Liu, H.; Tok, E. S.; Neto, A. H. C.; Özyilmaz, B.; Sow, C. H. Enhanced photoresponse from phosphorene−phosphorene-suboxide junction fashioned by focused laser micromachining. *Adv. Mater.* **2016**, *28*, 4090.
(16) Cao, L.; White, J. S.; Park, J.-S.; Schuller, J. A.; Clemens, B. M.; Brongersma, M. L. Engineering light absorption in semiconductor nanowire devices. *Nat. Mater.* **2009**, *8*, 643−647.
(17) Pettersson, H.; Trägårdh, J.; Persson, A. I.; Landin, L.; Hessman, D.; Samuelson, L. Infrared photodetectors in heterostructure nanowires. *Nano Lett.* **2006**, *6*, 229−232.
(18) Soci, C.; Zhang, A.; Xiang, B.; Dayeh, S. A.; Aplin, D. P. R.; Park, J.; Bao, X. Y.; Lo, Y. H.; Wang, D. ZnO nanowire uv photodetectors with high internal gain. *Nano Lett.* **2007**, *7*, 1003−1009.
(19) Li, P.; Appelbaum, I. Electrons and holes in phosphorene. *Phys. Rev. B: Condens. Matter Mater. Phys.* **2014**, *90*, 115439.
(20) Tran, V.; Soklaski, R.; Liang, Y.; Yang, L. Layer-controlled band gap and anisotropic excitons in few-layer black phosphorus. *Phys. Rev. B: Condens. Matter Mater. Phys.* **2014**, *89*, 235319.
(21) Liang, L.; Wang, J.; Lin, W.; Sumpter, B. G.; Meunier, V.; Pan, M. Electronic bandgap and edge reconstruction in phosphorene materials. *Nano Lett.* **2014**, *14*, 6400−6406.
(22) Novoselov, K. S.; Geim, A. K.; Morozov, S. V.; Jiang, D.; Katsnelson, M. I.; Grigorieva, I. V.; Dubonos, S. V.; Firsov, A. A. Two-dimensional gas of massless dirac fermions in graphene. *Nature* **2005**, *438*, 197−200.
(23) Zhang, Y.; Tan, Y.-W.; Stormer, H. L.; Kim, P. Experimental observation of the quantum hall effect and berry's phase in graphene. *Nature* **2005**, *438*, 201−204.
(24) Lu, J.; Liu, H.; Tok, E. S.; Sow, C.-H. Interactions between lasers and two-dimensional transition metal dichalcogenides. *Chem. Soc. Rev.* **2016**, *45*, 2494−2515.
(25) Li, Y.; Yang, S.; Li, J. Modulation of the electronic properties of ultrathin black phosphorus by strain and electrical field. *J. Phys. Chem. C* **2014**, *118*, 23970−23976.
(26) Mehboudi, M.; Utt, K.; Terrones, H.; Harriss, E. O.; Pacheco SanJuan, A. A.; Barraza-Lopez, S. Strain and the optoelectronic properties of nonplanar phosphorene monolayers. *Proc. Natl. Acad. Sci. U. S. A.* **2015**, *112*, 5888−5892.
(27) Horiuchi, N. Materials Science: Geometry and bandgaps. *Nat. Photonics* **2015**, *9*, 418−418.
(28) Rodin, A. S.; Carvalho, A.; Castro Neto, A. H. Excitons in anisotropic two-dimensional semiconducting crystals. *Phys. Rev. B: Condens. Matter Mater. Phys.* **2014**, *90*, 075429.
(29) Akahama, Y.; Endo, S.; Narita, S.-i. Electrical properties of black phosphorus single crystals. *J. Phys. Soc. Jpn.* **1983**, *52*, 2148−2155.
(30) Lin, J.-H.; Zhang, H.; Cheng, X.-L. First-principle study on the optical response of phosphorene. *Front. Phys.* **2015**, *10*, 1−9.
(31) Thilagam, A. Two-dimensional charged-exciton complexes. *Phys. Rev. B: Condens. Matter Mater. Phys.* **1997**, *55*, 7804−7808.
(32) Zhang, S.; Yang, J.; Xu, R.; Wang, F.; Li, W.; Ghufran, M.; Zhang, Y.-W.; Yu, Z.; Zhang, G.; Qin, Q.; Lu, Y. Extraordinary photoluminescence and strong temperature/angle-dependent raman responses in few-layer phosphorene. *ACS Nano* **2014**, *8*, 9590−9596.
(33) Xu, X.; Yao, W.; Xiao, D.; Heinz, T. F. Spin and pseudospins in layered transition metal dichalcogenides. *Nat. Phys.* **2014**, *10*, 343−350.
(34) Mak, K. F.; He, K.; Lee, C.; Lee, G. H.; Hone, J.; Heinz, T. F.; Shan, J. Tightly bound trions in monolayer MoS_2. *Nat. Mater.* **2013**, *12*, 207−211.
(35) Ross, J. S.; Wu, S.; Yu, H.; Ghimire, N. J.; Jones, A. M.; Aivazian, G.; Yan, J.; Mandrus, D. G.; Xiao, D.; Yao, W.; Xu, X. Electrical control of neutral and charged excitons in a monolayer semiconductor. *Nat. Commun.* **2013**, *4*, 1474.
(36) Xu, R.; Zhang, S.; Wang, F.; Yang, J.; Wang, Z.; Pei, J.; Myint, Y. W.; Xing, B.; Yu, Z.; Fu, L.; Qin, Q.; Lu, Y. Extraordinarily bound quasi-one-dimensional trions in two-dimensional phosphorene atomic semiconductors. *ACS Nano* **2016**, *10*, 2046−2053.
(37) Yang, J.; Xu, R.; Pei, J.; Myint, Y. W.; Wang, F.; Wang, Z.; Zhang, S.; Yu, Z.; Lu, Y. Optical tuning of exciton and trion emissions in monolayer phosphorene. *Light: Sci. Appl.* **2015**, *4*, e312.
(38) Huard, V.; Cox, R. T.; Saminadayar, K.; Arnoult, A.; Tatarenko, S. Bound states in optical absorption of semiconductor quantum wells containing a two-dimensional electron gas. *Phys. Rev. Lett.* **2000**, *84*, 187−190.
(39) Matsunaga, R.; Matsuda, K.; Kanemitsu, Y. Observation of charged excitons in hole-doped carbon nanotubes using photoluminescence and absorption spectroscopy. *Phys. Rev. Lett.* **2011**, *106*, 037404.
(40) Rodin, A. S.; Castro Neto, A. H. Collective modes in anisotropic double-layer systems. *Phys. Rev. B: Condens. Matter Mater. Phys.* **2015**, *91*, 075422.
(41) Nemilentsau, A.; Low, T.; Hanson, G. Anisotropic 2D Materials for Tunable Hyperbolic Plasmonics. *Phys. Rev. Lett.* **2016**, *116*, 066804.

DOI: 10.1021/acs.accounts.6b00266
Acc. Chem. Res. XXXX, XXX, XXX−XXX

(42) Sugai, S.; Ueda, T.; Murase, K. Pressure dependence of the lattice vibration in the orthorhombic and rhombohedral structures of black phosphorus. *J. Phys. Soc. Jpn.* **1981**, *50*, 3356−3361.
(43) Lu, W.; Nan, H.; Hong, J.; Chen, Y.; Zhu, C.; Liang, Z.; Ma, X.; Ni, Z.; Jin, C.; Zhang, Z. Plasma-assisted fabrication of monolayer phosphorene and its raman characterization. *Nano Res.* **2014**, *7*, 853−859.
(44) Favron, A.; Gaufres, E.; Fossard, F.; Phaneuf-Lheureux, A.-L.; Tang, N. Y. W.; Levesque, P. L.; Loiseau, A.; Leonelli, R.; Francoeur, S.; Martel, R. Photooxidation and quantum confinement effects in exfoliated black phosphorus. *Nat. Mater.* **2015**, *14*, 826−832.
(45) Ziletti, A.; Carvalho, A.; Campbell, D. K.; Coker, D. F.; Castro Neto, A. H. Oxygen defects in phosphorene. *Phys. Rev. Lett.* **2015**, *114*, 046801.
(46) Pei, J.; Gai, X.; Yang, J.; Wang, X.; Yu, Z.; Choi, D.-Y.; Luther-Davies, B.; Lu, Y. Producing air-stable monolayers of phosphorene and their defect engineering. *Nat. Commun.* **2016**, *7*, 10450.
(47) Xu, R.; Yang, J.; Myint, Y. W.; Pei, J.; Yan, H.; Wang, F.; Lu, Y. Exciton brightening in monolayer phosphorene via dimensionality modification. *Adv. Mater.* **2016**, *28*, 3493.
(48) Doganov, R. A.; O'Farrell, E. C. T.; Koenig, S. P.; Yeo, Y.; Ziletti, A.; Carvalho, A.; Campbell, D. K.; Coker, D. F.; Watanabe, K.; Taniguchi, T.; Neto, A. H. C.; Ozyilmaz, B. Transport properties of pristine few-layer black phosphorus by van der waals passivation in an inert atmosphere. *Nat. Commun.* **2015**, *6*, 6647.
(49) Yang, T.; Dong, B.; Wang, J.; Zhang, Z.; Guan, J.; Kuntz, K.; Warren, S. C.; Tománek, D. Interpreting core-level spectra of oxidizing phosphorene: Theory and experiment. *Phys. Rev. B: Condens. Matter Mater. Phys.* **2015**, *92*, 125412.
(50) Wood, J. D.; Wells, S. A.; Jariwala, D.; Chen, K.-S.; Cho, E.; Sangwan, V. K.; Liu, X.; Lauhon, L. J.; Marks, T. J.; Hersam, M. C. Effective Passivation of Exfoliated Black Phosphorus Transistors against Ambient Degradation. *Nano Lett.* **2014**, *14*, 6964−6970.
(51) Utt, K. L.; Rivero, P.; Mehboudi, M.; Harriss, E. O.; Borunda, M. F.; Pacheco SanJuan, A. A.; Barraza-Lopez, S. Intrinsic defects, fluctuations of the local shape, and the photo-oxidation of black phosphorus. *ACS Cent. Sci.* **2015**, *1*, 320−327.
(52) Edmonds, M. T.; Tadich, A.; Carvalho, A.; Ziletti, A.; O'Donnell, K. M.; Koenig, S. P.; Coker, D. F.; Özyilmaz, B.; Neto, A. H. C.; Fuhrer, M. S. Creating a stable oxide at the surface of black phosphorus. *ACS Appl. Mater. Interfaces* **2015**, *7*, 14557−14562.
(53) Lu, J.; Wu, J.; Carvalho, A.; Ziletti, A.; Liu, H.; Tan, J.; Chen, Y.; Castro Neto, A. H.; Özyilmaz, B.; Sow, C. H. Bandgap engineering of phosphorene by laser oxidation toward functional 2d materials. *ACS Nano* **2015**, *9*, 10411−10421.
(54) Lou, Z.; Li, L.; Shen, G. High-performance rigid and flexible ultraviolet photodetectors with single-crystalline znga2o4 nanowires. *Nano Res.* **2015**, *8*, 2162−2169.
(55) Albrecht, B.; Kopta, S.; John, O.; Kirste, L.; Driad, R.; Köhler, K.; Walther, M.; Ambacher, O. AlGaN ultraviolet A and ultraviolet C photodetectors with very high specific detectivity D*. *Jpn. J. Appl. Phys.* **2013**, *52*, 08JB28.
(56) Low, T.; Rodin, A. S.; Carvalho, A.; Jiang, Y.; Wang, H.; Xia, F.; Castro Neto, A. H. Tunable optical properties of multilayer black phosphorus thin films. *Phys. Rev. B: Condens. Matter Mater. Phys.* **2014**, *90*, 075434.
(57) Seixas, L.; Rodin, A. S.; Carvalho, A.; Castro Neto, A. H. Exciton binding energies and luminescence of phosphorene under pressure. *Phys. Rev. B: Condens. Matter Mater. Phys.* **2015**, *91*, 115437.
(58) Ziletti, A.; Carvalho, A.; Trevisanutto, P. E.; Campbell, D. K.; Coker, D. F.; Castro Neto, A. H. Phosphorene oxides: Bandgap engineering of phosphorene by oxidation. *Phys. Rev. B: Condens. Matter Mater. Phys.* **2015**, *91*, 085407.

DOI: 10.1021/acs.accounts.6b00266
Acc. Chem. Res. XXXX, XXX, XXX−XXX